SHALLOW-LANDSLIDE SPATIAL STRUCTURE INTERPRETATION USING A MULTI-GEOPHYSICAL APPROACH

ALEKSANDAR RISTIĆ, BILJANA ABOLMASOV, MIRO GOVEDARICA, DUŠAN PETROVAČKI and ALEKSANDRA RISTIĆ

about the authors

Aleksandar Ristić
University of Novi Sad,
Faculty of technical sciences
Trg Dositeja Obradovića 6, 21000 Novi Sad, Serbia
E-mail: aristic@uns.ac.rs

Biljana Abolmasov
University of Belgrade,
Faculty of Mining and Geology
Đušina 7, 11000 Beograd, Serbia
E-mail: biljana@rgf.bg.ac.rs

Miro Govedarica
University of Novi Sad,
Faculty of technical sciences
Trg Dositeja Obradovića 6, 21000 Novi Sad, Serbia
E-mail: miro@uns.ac.rs

Dušan Petrovački
University of Novi Sad,
Faculty of technical sciences
Trg Dositeja Obradovića 6, 21000 Novi Sad, Serbia
E-mail: petrovacki@uns.ac.rs

Aleksandra Ristić
University of Novi Sad,
Faculty of technical sciences
Trg Dositeja Obradovića 6, 21000 Novi Sad, Serbia
E-mail: sanjica@uns.ac.rs

Abstract

We present an methodology for a more detailed and less ambiguous spatial structure interpretation of small, shallow landslides. The spatial structure interpretation of this type of landslides bases on both underground and surface models and requires high-density data. This methodology involves the use of ground-penetrating radar (GPR), electrical resistivity tomography (ERT) and terrestrial laser scanning (TLS) techniques. GPR technique, used for the definition of the underground structure model, provides a time-efficient survey that yields high-resolution data, making it suitable for a shallow subsurface analysis. ERT technique was used only to confirm the results obtained by the GPR survey, since it is more time consuming and more convenient for larger and deeper landslides investigations. The surface model is created using TLS technique, which is time- and cost-effective, produces a large amount of data and is favourable for smaller areas, such as the analysed type of landslides.

To the best of the authors' knowledge, existing procedures based on either conventional or non-invasive geophysical methods, observe, almost exclusively, larger and deeper landslides. Their real-time monitoring involves a number of sensors and is hardly applicable to small landslides because of their number, location and dimensions. Considering the benefits of each applied technique and the interpretation of the results obtained from field data, it is clear that the main advantages of the realized application are the efficiency and applicability for small shallow landslides whose number and impact on the environment are dominant. Therefore, it represents a solid basis for landslide mitigation.

The verification of the methodology was made on a small, shallow landslide in the village of Vinča, near Belgrade, Serbia.

keywords

shallow landslide, GPR, ERT, TLS

1 INTRODUCTION

Determining the characteristics of the underground and surface structures of landslides represents the principal result necessary for an adequate assessment of the status and monitoring of landslide activities [1]. The conventional methods for landslide-status assessment are based on geo-morphological analyses, in most cases combined with borehole drilling and standard penetration test (SPT) methods. Conventional methods are expensive and relatively slow, whereas the results of an analysis are based on processing a limited range

of subsurface data [2]. These disadvantages may be overcome by the combined or independent application of non-invasive, geophysical methods whose expansion follows the development of modern techniques and instruments [3]. Simultaneously with the development of these methods, the possibilities for their application in the detailed research of landslides were analysed [2,4]. These analyses were carried out almost exclusively for large landslides with a sliding depth greater than 20m, and showed that ERT technology is appropriate in these conditions [5,6,7,8,9,10].

ERT measurements are conducted by applying a constant current into the ground through two current electrodes and measuring the resulting voltage differences at two potential electrodes. From the current and voltage values, an apparent resistivity value is calculated. ERT uses 25 or more electrodes connected by a multicore cable. To determine the subsurface resistivity in different zones or layers, an "inversion" of the measured apparent resistivity values (generally a total of some 100 single values) must be carried out. The result gives information about the spatial averages of the subsurface resistivity in a 2D-section. The main disadvantage of the ERT method is the wide range and the broad overlap of the possible subsurface resistivity of different geological units. Thus, resistivity changes due to varying moisture conditions may be orders of magnitude higher than the differences between geological units [1,9,15].

In terms of large, deep landslides, GPR technology has only been used to confirm the results of ERT technology, due to maximum penetration depth of electromagnetic (EM) waves and the site accessibility [2].

The GPR method is used for the very shallow subsurface, i.e., of the order of a few tens of metres. The technology is based on an EM pulse emitted from a transmitter antenna, reflected at inhomogeneities and layer boundaries and received by a second antenna after a measured travel time. The whole array is moved along a profile line, which creates a 2D-section of the subsurface called the B-scan. The possible antenna frequencies range from 20MHz to 2GHz. A higher antenna frequency enhances the resolution of the data, while lower frequencies increase the maximum penetration depth. In the frequency range used for geological investigations, GPR signals can reach depths of up to 20 m with 100-MHz antennas, but the signal penetration decreases dramatically with the increasing soil conductivity. Because of the high dielectric constant of water, this method is well suited for detecting changes in water content [2,3,9,17].

Considering that the main goal of the research is to determine the characteristics of small, shallow landslides with a sliding depth in the range from 1 to 5m, then the application of GPR technology, which is characterized by the swift and completely non-invasive acquisition of high-resolution data, becomes very appropriate [11]. Taking into account the possibilities for non-invasive geophysical methods, they are rarely carried out independently. More often, they are used in combination with other methods and then a correlation of the obtained results is carried out. Such a multi-geophysical approach of using different methods combined with traditional methods of research is described in various articles [12,13]. The advantages and disadvantages of using geophysical methods in geomorphological studies are described on various examples in [14].

In addition to various field and laboratory research methods that define the structure and properties, it is appropriate to provide a topographic basis on a large scale. When research is more detailed, such a topographic basis is necessary in order to define the landslide geometry and the procedure of landslide mitigation. Conventional methods for a geodetic survey are used to provide a topographic basis in most practical cases. Occasionally, terrestrial photogrammetry [15] and terrestrial laser scanning of the terrain [16,17] were used.

A laser scanner is a system that scans real objects to produce three-dimensional, discretely sampled surfaces that represent those real objects. Scanning can be airborne (ALS) or terrestrial (TLS). Laser scanning allows the generation of high-resolution, digital surface models (DSM), which is a topographic model of the reflected surface of the earth, including vegetation and man-made structures, and digital terrain models (DTM), which is a topographic model of the bare earth. Elevation data collected by TLS have proven to be useful in the determination of some specific landform features, such as landslides and fault scarps [5,16,17].

On the basis of previously mentioned points, it can be concluded that the recent results of landslide analyses point to a multi-geophysical approach. Also, the structure analysis of small, shallow landslides was rarely tackled in the available literature, while GPR technology was not applied to any great extent.

The given analysis, along with the defined main goal of the research, leads to the conclusion that it is necessary to realize an application based on the usage of the main advantages of the GPR, ERT and TLS technologies. The application then has to be verified on a typical landslide example.

During the research the emphasis was put on non-invasive geophysical methods since a landslide has a specific

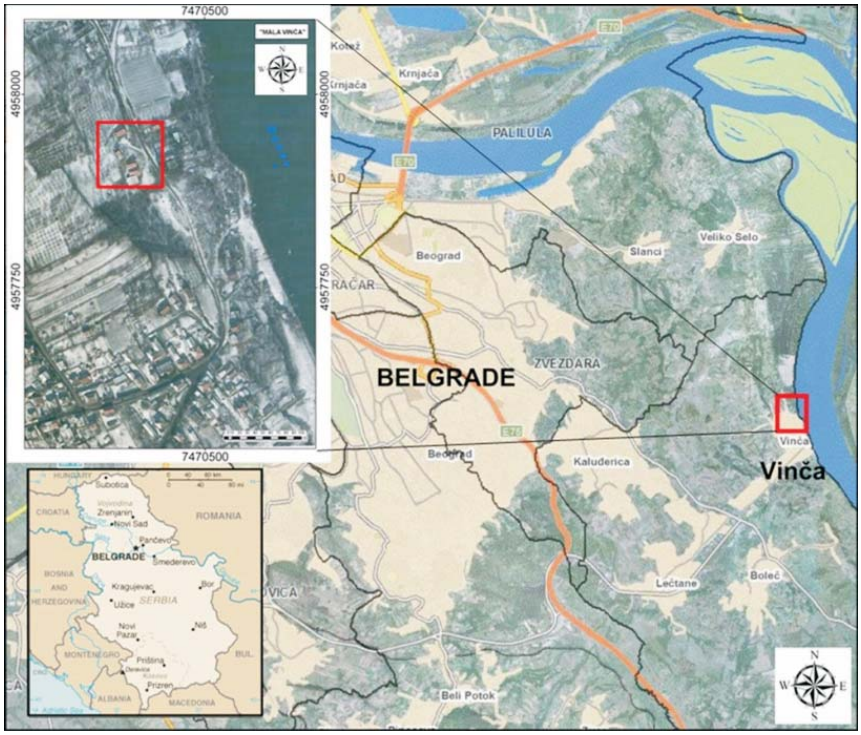

Figure 1. Location of the study area.

position and geometry. Due to the capabilities of non-invasive geophysical methods for landslide research [2], field work was conducted during the summertime (July 2009), in a dry period, after a period of heavy precipitation in the previous winter and spring, which reactivated the landslide. The results presented in this paper clearly show that in the case of small, shallow landslides, applied geophysical methods give reliable data about the structure of a landslide body and the spatial disposition of the rupture surface. The TLS scanning of the landslide surface provided a topographic basis for creating DTMs, locating the research work and monitoring the landslide activities.

2 STUDY AREA

The integrated geophysical research was carried out on a landslide located 14km southeast of Belgrade, in the village of Vinča, on the right bank of the Danube (Fig. 1). The right valley bank of the Danube is characterized by hills (altitude 80–130m) and numerous deep landslides whose feet reach the Danube [18]. The geological composition of the study area (Fig. 2) includes a continuous surface layer of diluvium (dl) with a thickness of 0.2–0.5m and beneath it there is loess (Q) with a

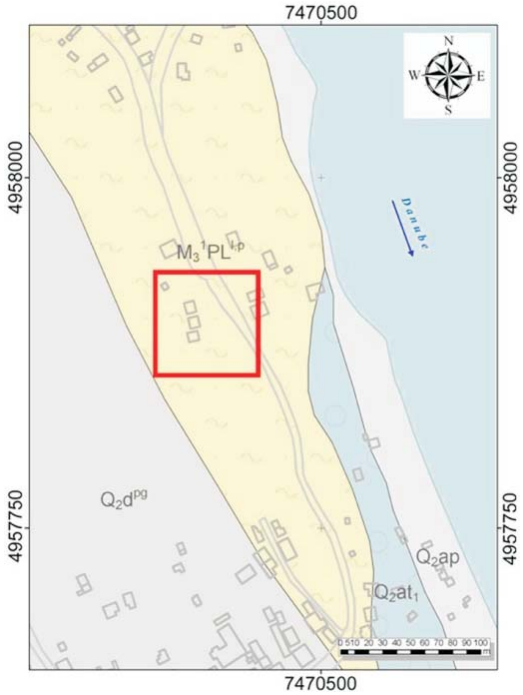

Figure 2. Complex geological map of Belgrade 1:10000 [19]. Legend: Q_2at_1 - Fluvial terrace (first), Q_2ap - Alluvial sediments, Q_2d^{pg} - Deluvial dusty-sandy-clayish deposits, $M_3{}^1PL^{l,p}$-Sarmatian dusty-clayish formation.

thickness of 0.5–2.0m, with traces of secondary carbonate sediments. The bedrock consists of Sarmatian sand (M_3^1), brownish marlstone (M_3^1GL) and grey marlstone (M_3^1L).

The analysed landslide has the dimensions of 50x40m and it is situated in the middle of the Danube slope above the local road and three private residential objects that are directly endangered by the landslide (Fig. 1, Fig. 2). The landslide is on private property and, due to the specific terrain configuration and the problems with the owners of nearby properties, it is almost impossible to reach the body of the landslide equipped with drill tools and tools for SPT experiments.

The landslide activated in March 2008 was triggered by heavy rainfall and slope indentation. The indentation occurred while building the residential objects. The first reactivation occurred in March 2009 (Fig. 3), also triggered by heavy rainfall. The second reactivation occurred in late December 2009 and was triggered by instant snow melting. According to classification [20], this landslide can be classified as a shallow retrogressive and active landslide, very slow to slow, in the phase of active movement. The main scarp, with a height of 1.7m, is obvious with the visible zone of mass deficit. The lithological structure of the landslide comprises a thin diluvium with a thickness up to 0.3m, loess with a thickness of 1–1.5m and bedrock consisting of Sarmatian, laminated, well-compacted sand with weathered marlstone.

3 SURVEY PROCEDURE

The geological recognition of the landslide was conducted in March 2009, then again during the research in July 2009, and finally after the reactivation in December 2009. The pre-failure DTM was formed on the basis of the available cartographic material for the study area prior to the formation of the landslide.

3.1 TERRESTRIAL LASER SCANNING

The acquisition was made in July 2009 with a Leica Scan Station 2 terrestrial laser scanner (scanning resolution 10cm/10m). The raw data were processed and used as input data for the topographic map and the post-failure DTM time series 1. The point cloud was formed by scanning from four different positions of the scanner, and it covers an area of about 2200m^2, composed of the landslide itself and the nearby area. The data processing was done in order to eliminate the errors of the measurement and to classify the points belonging to the ground, buildings and trees. The resulting topographic map and DTM time series 1 were used to geo-reference the data collected by all the used technologies, and for the purpose of calculating the landslide volume [17,21]. Fig. 4a shows DTM time series 1 in the form of a triangle irregular network (TIN) with contour lines (continuous black and green lines) and with the positions of the laser scanner during the acquisition (bolded black circles marked B1 to B4). In Fig. 4b is the rendered TIN view of the landslide with its basic geometric characteristics.

Figure 3. Photo of landslide in Vinča – March 2009.

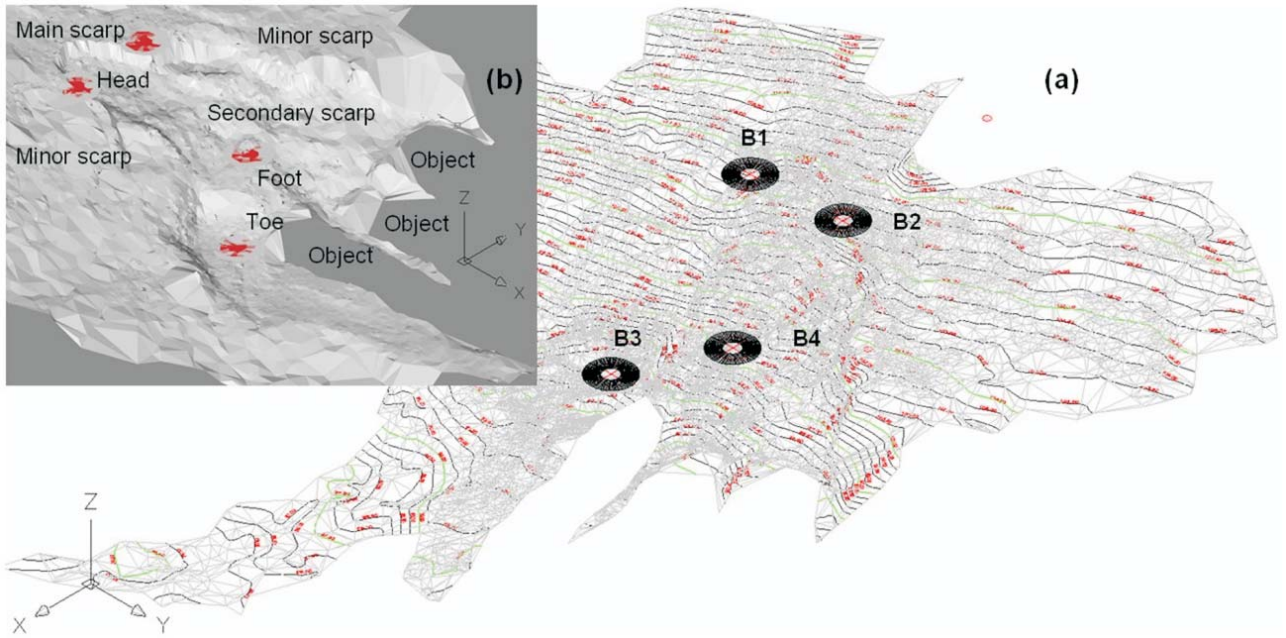

Figure 4. DTM time series 1 with characteristic elements of the landslide.

After a second reactivation of the landslide in December 2009, scanning with a terrestrial laser scanner(Leica Scan Station 2) was carried out in April 2010, and a post-failure DTM time series 2 was produced. The comparative analysis of the DTM time series 1 and 2 defines the landslide volume during the second reactivation.

3.2 GROUND-PENETRATION RADAR SCANNING

The data acquisition was carried out in July 2009 with the GSSI SIR3000 system. The formation of B scans was carried out using antennas with a central frequency of 200, 400 and 900MHz and a high scan resolution of 1024 samples/scan, and 100 scan/m. The maximum scanning depth of 4m was achieved by an antenna with a central frequency of 200MHz, taking into consideration the soil structure in the landslide body and the capabilities of used antenna. The GPR calibration, in terms of determining the dielectric constant of soil, was made according to the known lithological structure of the main scarp area [11,22]. It was created with 30 B scans labelled from F029 to F059, on and around the landslide body. Fig. 5 shows the layout of the B scans selected for further discussion. The B scans are represented with the direction of the antenna motion (marked by arrow) and the label. The points used to geo-reference the B scans were measured using two Trimble 5800 Global Positioning System (GPS) rovers in Real-Time Kinematic (RTK) mode (first covers the points 01–16, while the second covers the points p001–p011). The set of characteristic points for the B scan geo-referencing contains a start and end point. The B scan post-processing, conducted with the software package RADAN, included a determination of the time zero distance (the distance from the antenna centre to the soil surface), and the application of several digital signal-processing algorithms for reflected signals' processing. It was done in order to obtain a clear view of all the structural characteristics of landslides [11,22].

3.3 ELECTRICAL RESISTIVITY TOMOGRAPHY

In addition to the acquisition by GPR, another profile of detailed ERT scanning was done and its location is shown by the discontinuous line in Fig. 5. The equipment used for the data acquisition was an ABEM SAS 300B with a sensitivity of 0.01mV. The length of the profile was 45 metres, and there was 113 points at 6 depth levels. The distance between two measuring points (step) was 2m, while the total depth was approximately 4m. The processing of the measured data was conducted

using the software packet RES2DINV. The complete profile was carried out by a combination of Wenner-Schlumberger array electrodes. The first depth level was made using theWenner array configuration; the distances between A-M-N-B were equal (2m), whereas A and B are electrodes for introducing electric current J (mA) into the ground, and M and N are electrodes for measuring the difference in the electric potential ΔV(mV). From the level 2 to level 6 electrode configuration thee Schlumberger was used, where the distance M-N remains the same (2m) while the distance between the current electrodes A-B successively increases (10, 14, 18, 22 and 26 m). The measurements on the points consisted of placing M and N at a distance of 2 metres, and a series of measuring ΔV/J ratio at the increasing distances A and B from 6m (Wenner, 2-2-2) to 26m (Schlumberger, 12-2-12, for last sixth level). In case of the Schlumberger configuration A-M-N-B, A-M and N-B, the distances between the electrodes increased successively (2, 4, 6, 8, 10 and 12m).

4 RESULTS AND DISCUSSION

4.1 GEOPHYSICAL RESULTS

Using the technologies of GPR and ERT, 31 profiles are generated: 30 GPR profiles and 1 ERT profile. Several GPR profiles that characterize the most important features have been selected for discussion. The interpretation and relation of the geophysical data to the lithological data are then presented in the following.

The disposition of the B scans F032, F033 and F034 and its starting and ending points (formed in nearby, undisturbed terrain) is shown in Fig. 5. Lithological elements that can be found in the landslide body are noticed in these B scans as well. The marks from 1 to 4 define the positions of the borders between the soil horizons in these B scans. The horizontal axis in the B scan represents the sequence of EM wave reflections recorded during the antenna movement. The number of these reflections depends on the travelled distance and the scanning resolution (the number of reflections per distance unit). For this research we used 100scans/1m resolution. The vertical axis in the B scan represents the depth of the recorded layers in meters. Initially, GPR records the two-way travel time in nanoseconds for each anomaly in one reflection. Then, from these values the depth in meters is calculated, considering the soil characteristics described with the dielectric constant εR. The borders between the soil horizons in the B scan correspond to the local maximum values of the reflections. If these values are determined for each reflection in the B scan then the border line between the soil horizons can be formed.

4.1.1 Right-side scarp

The B scan F032, 16m[1] long, is formed in undisturbed terrain, about 1m parallel to the edge of the right side scarp (Fig. 5). The coordinates of the beginning of the B scan F032 (0m[1]) are not measured by GPS (surrounded by trees), and the end of the B scan corresponds to the point 07 (16m[1]). The changes in terms of the phase inversion of the reflected signal and the disorder of the structure range from 7m[1] to 16m[1] (Fig. 6). The changes are especially visible from 7m[1] to 12m[1].

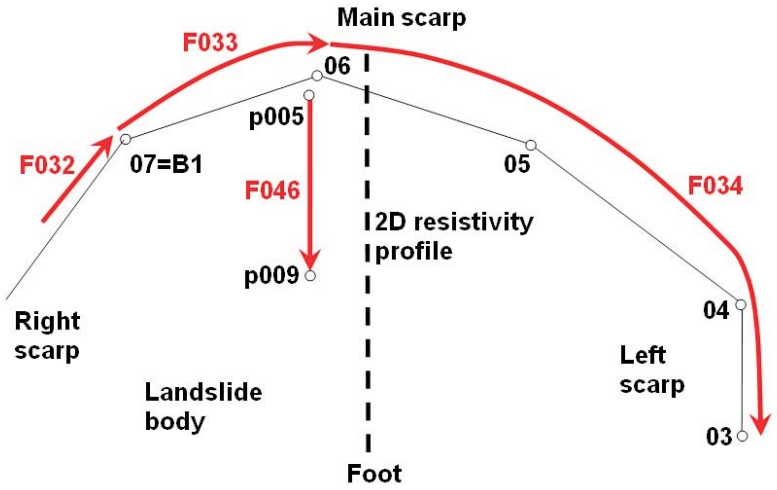

Figure 5. Disposition and parameters of the acquisition for the B scans (red line) and the ERT profile (dashed line). Thin black line represents the landslide edges.

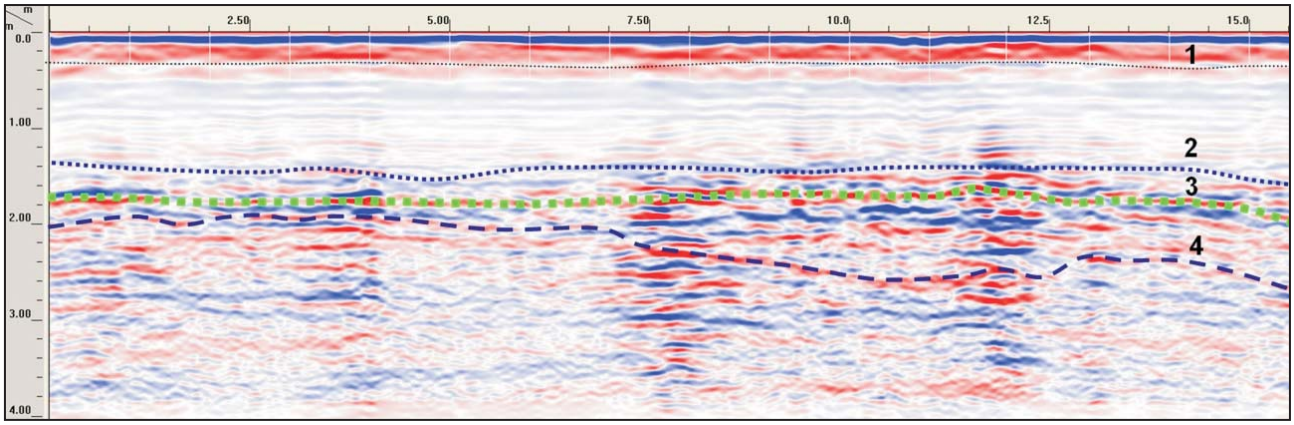

Figure 6. Interpretation of the B scan F032 on the right-side scarp.

4.1.2 Head scarp apex

The B scan F033, 7m[1] long, is formed in undisturbed terrain left from the head scarp apex (Fig. 5). The beginning of the F033 B scan (0m[1]) corresponds to the coordinates of the point 07 (the position of the scanner B1), and the end of the B scan corresponds to the point 06 (7m[1]) – the head scarp apex (Fig. 7a). The scanning resolution in the B scan F033 was 100scan/1m. In Fig. 7a scan 390 (at 3.9m from starting point 07) is represented by an oscilloscope preview of the reflected signal with clearly visible borders between the soil horizons (local maximum values of the reflection 390).

Since it was possible to see a part of the soil horizons on the main scarp apex, they served as a solid basis for interpreting the geophysical data. Therefore, the B scan F033 is formed directly above the scarp, so the geophysical parameters can be defined and correlation between the borders in the B scan and the visible soil horizons are established. Fig. 7b shows a visual representation of the borders 2 and 3, which served as a basis for the recalibration of a device and defining the dielectric constant ε_R=28 [23].

4.1.3 Head scarp apex – left-side scarp

The B scan F034, 33m[1] long, is formed in undisturbed terrain (at the time of acquisition) and involves the entire left-side scarp starting from the head scarp apex (Fig. 5). The beginning of the B scan F034 (0m[1]) corresponds to the coordinates of the point 06, 8m[1] corresponds to the point 05, 24m[1] to the point 04, and the end corresponds to the point 03 (33m[1]). The changes in

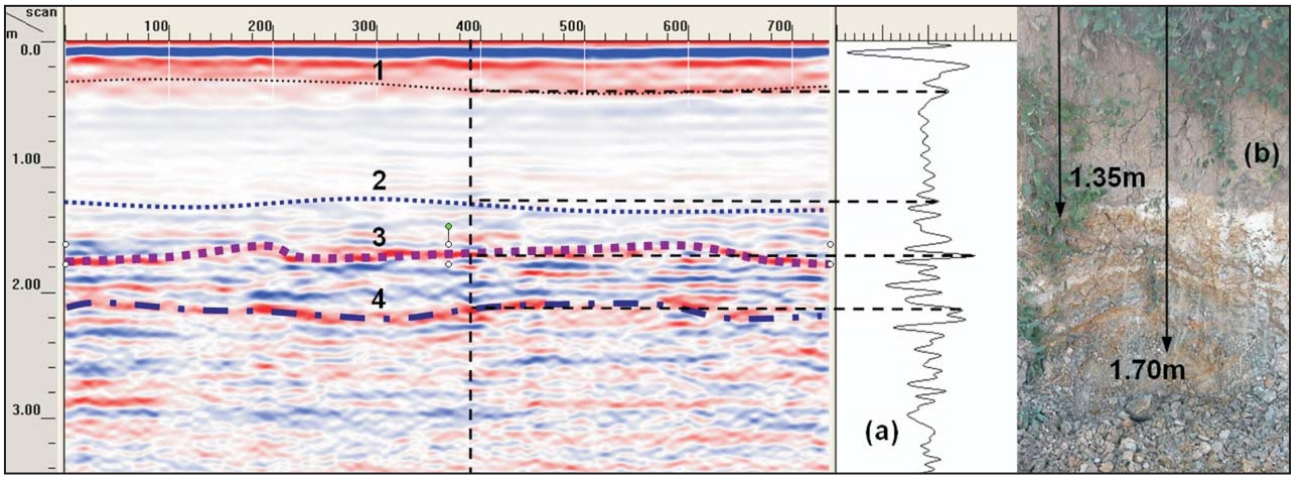

Figure 7. Interpretation of B scan F033 on the head scarp apex.

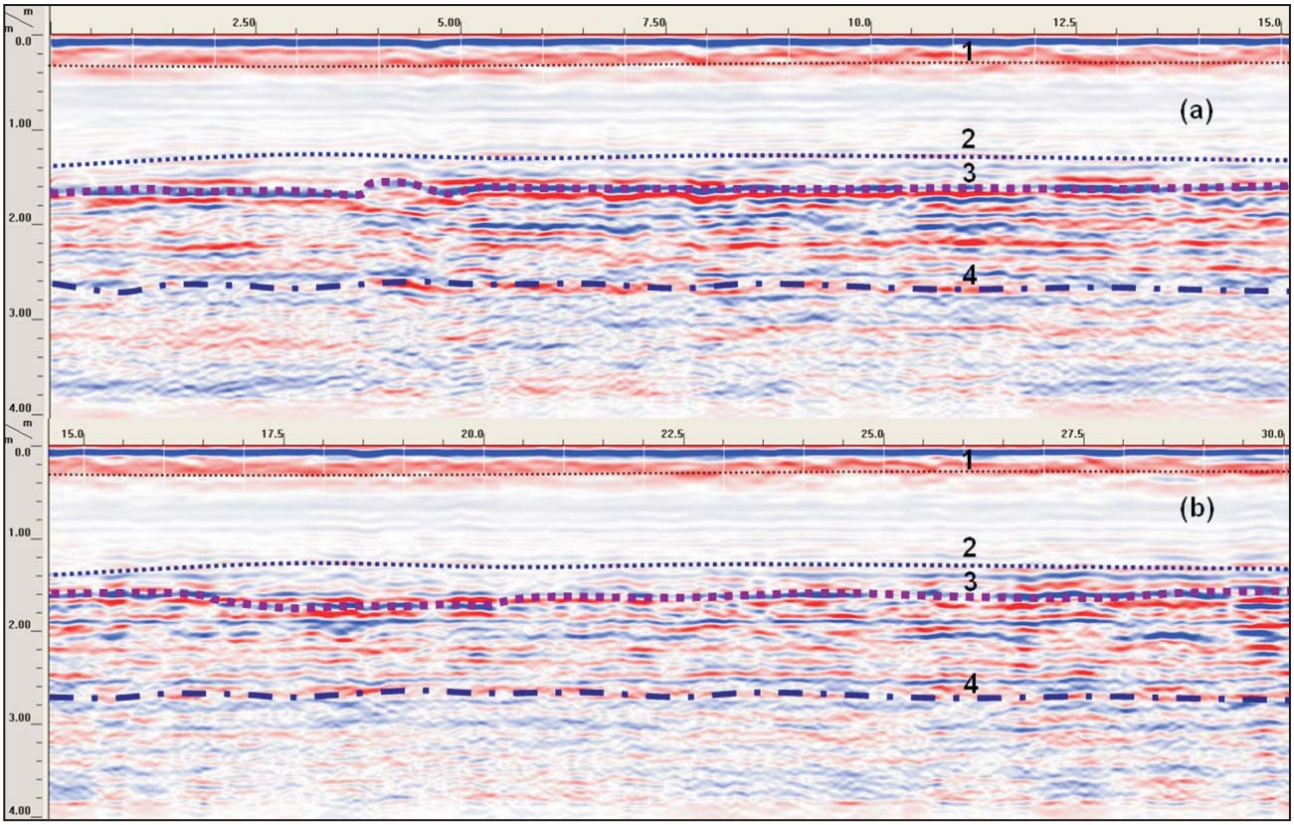

Figure 8. Interpretation of B scanF034 on the head scarp apex – left side scarp.

terms of the phase inversion of the reflected signal and the disorder of the structure can be seen in a complete B scan (Fig. 8a and 8b). The changes are especially noticeable from $2m^1$ to $20m^1$.

The interpretation of the B scans F032, F033 and F034 (Fig. 6, 7 and 8)

- Soil horizon from the surface to the border 1 – from 0 to 30cm – humificated loess diluvium, dark brown, dry
- Soil horizon between borders 1 and 2 – from 30 to 135cm – loess diluvium, pale brown, dry with variable amount of carbonates
- Soil horizon between borders 2 and 3 – from 135 to 170cm – incoherent sand, pale brown
- Soil horizon between borders 3 and 4 – from 170 to 210cm – on F032, that is, 260cm on F034 – altered marlstone; at 170 cm there is maximum reflected amplitude, probably clay sediments but also distorted structures and air-filled fractures, which was confirmed after the second reactivation of the landslide in December 2009 (Fig. 9)
- Soil horizon beneath border 4 – high reflection amplitude, probably weak consolidated sand, no phase inversion and a small amount of moisture.

Figure 9. Detail of distorted structure of marlstones in the left side scarp (photo December 2009).

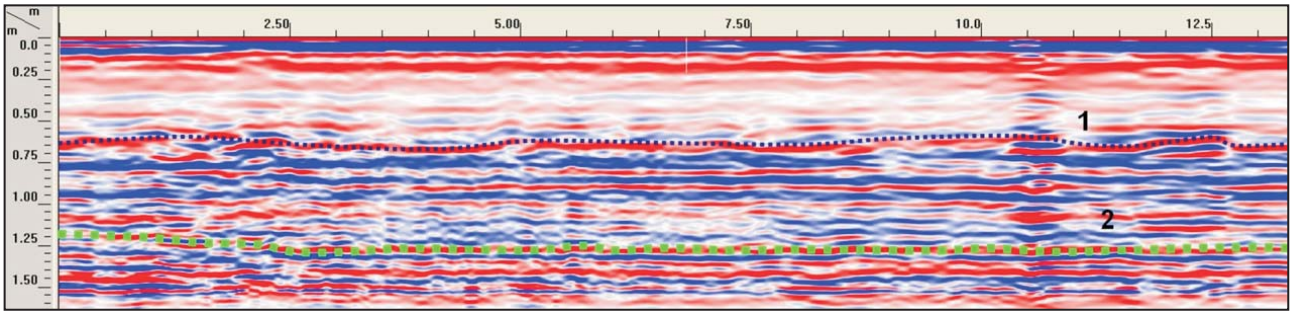

Figure 10.Interpretation of B scan F046 – central cross section, landslide body.

4.1.4 central cross section – in landslide body

The B scan F046, 13.6m[1] long, is formed in the landslide body starting from the head scarp apex to the centre of the landslide body (Fig. 5). The beginning of B scan F046 (0m[1]) corresponds to the point p005, and the end of the B scan corresponds to the point p009 (13.6m[1]) (Fig. 10). The trace of the B scan F046 overlaps part of the ERT profile (Fig. 11), where the starting point of the B scan p005 corresponds to 37m[1] of the ERT profile, and the ending point of the B scan p009 corresponds to 23m[1] of the ERT profile. Since the height of the starting point p005 is 113.9m above mean sea level and the end point p009 is at 109.4m, then the difference in height of the profile is 4.5m.

The comparative analysis of the geophysical data from the common parts of the B scan trace F046 and ERT profile showed an excellent correlation. It is explained in more detail when interpreting the results from the ERT profile.

The labels 1 and 2 define the position of the interpreted borders on the B scan F046:

- Soil horizon from the surface to the border 1 – from 0 to 65cm – homogenous lithological composition and structure
- Soil horizon between borders 1 and 2 – from 65 to 120cm – disorder in structure and phase inversion of reflected signal
- Soil horizon beneath border 2 – completely disordered structure with a high percentage of clay and significant attenuation of the signal. Possible surface of the rupture is expected in this soil horizon, but deeper than the maximum penetration depth of the EM wave.

4.1.5 ERT profile - central cross-section in landslide body

In the raw ERT profile (Fig. 11a) three resistivity zones can be identified [9, 13, 15]. First, there is a clearly visible zone with a low specific electrical resistivity with values between 10 and 20 Ωm (marked with shades of blue colour). This zone reaches a depth of 65cm and it can be related to moved diluvium and loess sediments and incoherent sands.

Second, the resistivity zone with values between 20 and 70 Ωm (in the ERT profile marked with shades of green), can be related to the landslide body consisting of moved diluvium, loess and sand, and at the bottom there is marlstone where, at a depth of maximum 170cm, the surface of rupture was formed.

The third, clearly identified, resistivity zone in ERT profile was coloured in yellow to the nuances of red with corresponding resistivity ranging from 70 to 250 Ωm. This zone most probably corresponds to weak consolidated sand that can be seen in immediate adjacency to the landslide on a smaller vertical cut. Also, there are traces of clay.

In ERT profile the debris can be distinguished, i.e., the material that is deposited from 0m[1] to 10m[1] of the profile length.

According to the identified resistivity values a re-interpretation was made and the resistivity zones became more visible (Fig. 11b).

Comparing the interpretation results of the B scan F046 and the ERT profile it can be seen that border 1 on the B scan corresponds to the resistivity zone 1 on the ERT profile. Also, border 2 on the B scan corresponds to the

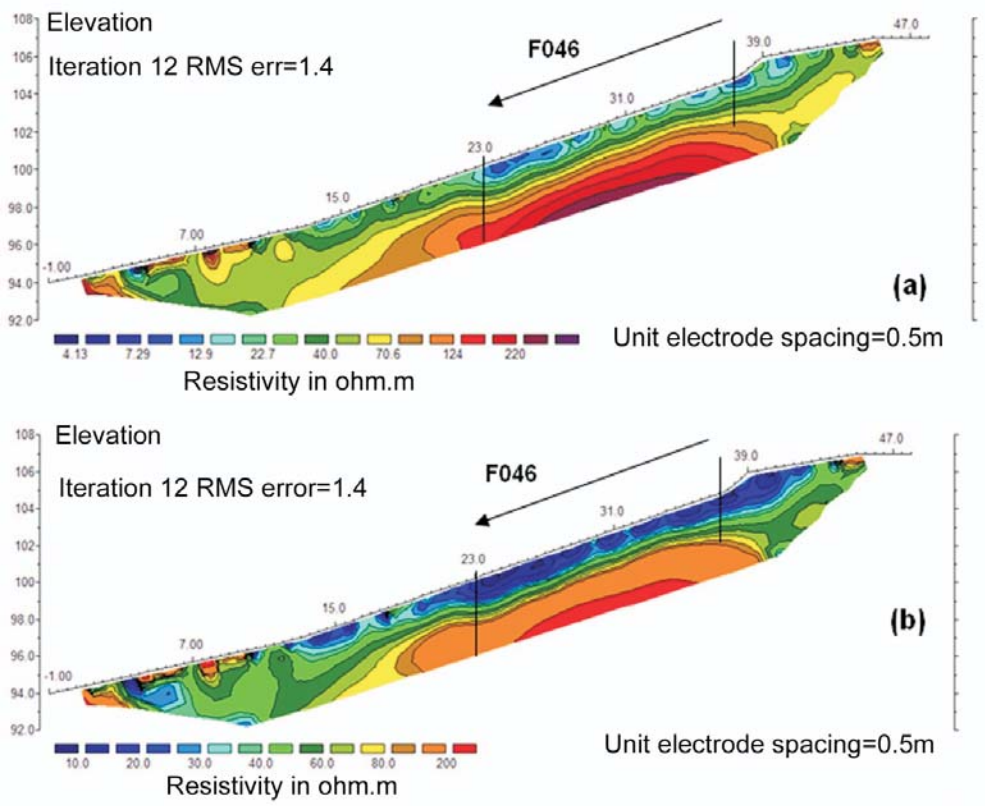

Figure 11. Interpretation of the ERT profile.

light-green colour from resistivity zone 2 on the ERT profile. It means, in this case, these two methods resulted in well-correlated data.

The ERT profile is perpendicular to head scarp and crosses the B scans F033 and F034. Since there is an overlapping zone above the head scarp apex it is possible to compare the interpretation results of the B scans and the profile. There are overt changes in the soil structure in a length of maximum 3m[1] (from 39m[1] to 42m[1] in ERT profile) and to a depth of maximum 170cm that can be noticed on the B scans as well. This leads to the conclusion that in this zone it is expected to have a further expansion of the landslide. After the landslide reactivation in December 2009 this assumption was confirmed. Reactivation occurred in zones of the left-side and head scarp. The surface of the rupture was revealed at the depth of 170–180cm (Fig. 12).

4.2 DTM ANALYSIS

In Fig. 13a DTM time series 1 is represented in cyan colour, and it includes the landslide body and the zone around the landslide. It was created by terrestrial laser scanning in July 2009, a year and so after the landslide activation (March 2008), and a few months after the first reactivation (March 2009). The DTM time series 1 is used to geo-reference all the data obtained by the acquisition in the field, as well as for the calculation of

Figure 12. Revealed surface of rupture after the landslide reactivation in December 2009.

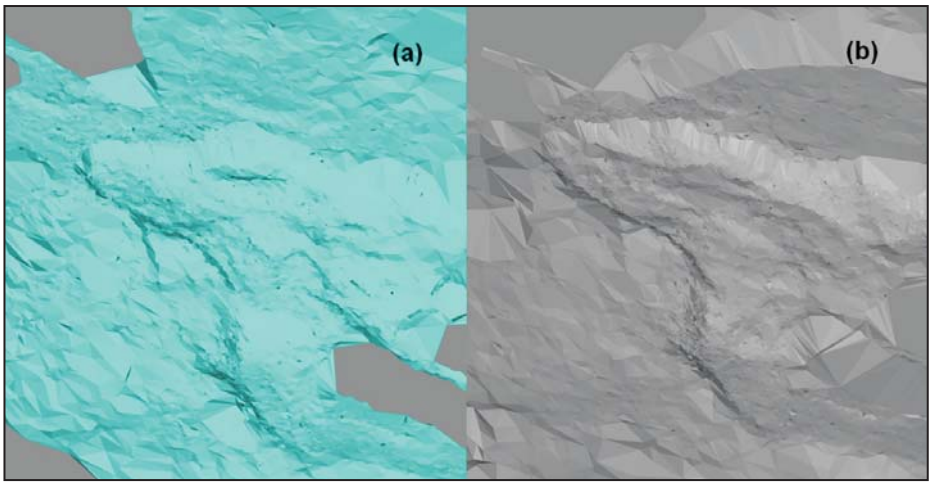

Figure 13. DTM time series 1 and 2.

the landslide volume from the moment of the landslide activation to the time of the first scanning in July 2009. The results of the comparative geometric analysis of time series 1 and the pre-failure DTM showed that the landslide volume was 1219m^3 [17].

Since in late December 2009 the second reactivation occurred in zones of the left-side and head scarp, a new data acquisition was made in April 2010 by terrestrial laser scanning with the same geo-referencing parameters. The aim of the second scanning was to monitor the movement of the material between the first and second reactivation of the landslide and to determine the differences in the dimensions of the landslide. The DTM time series 2 formed as represented in the grey in Fig. 13b. The results of the comparative geometric analysis of the DTMs time series 1 and 2 [17] showed that a new 117m^3 was moved, and that the total landslide volume was 1336m^3.

Fig. 14 shows a comparative representation of the DTM time series 1 and 2. It can be clearly seen that there is a movement of material in the top zone of left-side scarp and the main scarp. The DTM time series 1 is repre-

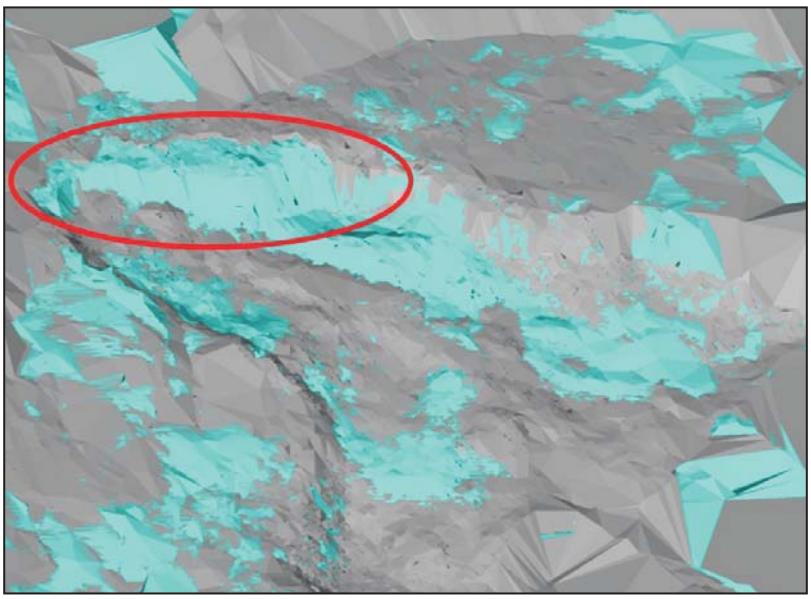

Figure 14. DTM time series 1 and 2 – comparative representation.

sented in cyan, whereas the DTM time series 2 is shown in grey. There are some variations of the DTM in the landslide body due to discarding the moved material by the owner of the building objects at the bottom.

If the final results of the geophysical research in the zone landslide are integrated with the results obtained by comparative analysis of the DTM time series 1 and 2, there is an evident tendency of movement of material at the top part of the left-side scarp.

5 CONCLUSIONS

The spatial structure interpretation of small, shallow landslides was analysed in this paper. The characteristics of these landslides require high-density data, while their number and size demands ground-based technologies able to collect a large amount of data in a short time. Considering the capabilities of existing technologies the landslide spatial structure has to be divided into surface and underground models. Therefore, an application for spatial structure interpretation should be based on a multi-geophysical approach.

Our application combines GPR, ERT and TLS technologies and it has been successfully verified on a typical example of the landslide in the village of Vinča, near Belgrade. GPR technology was chosen for a definition of the underground structure model, since it provides a time-efficient survey and high-resolution data. The ERT data were used as control data for the GPR results, because the ERT technology is slow and convenient for larger and deeper landslides. The most important results include estimation of the surface of the rupture at the depth of 1.70m, the composition of the landslide body and the prediction of the landslide enlargement directions.

The surface model is represented as a DTM created using TLS technology, which appeared to be most appropriate considering the small, shallow, landslide dimensions, accessibility and vegetation. The DTMs are obtained in pre- and post-failure time series. A comparative analysis of the DTMs provided the data on the total landslide volume of 1336m^3. The geophysical data are interpreted on the basis of a lithological analysis as well as the analysis of DTMs used to monitor the activities of the landslide. The conclusions derived from an interpretation of the GPR data were confirmed by the DTM analysis by means of landslide enlargement directions.

The technology used for real-time monitoring of large and deeper landslides involves a number of sensors and it is hardly applicable to small ones because of their number, location and dimensions. Therefore, the technology for periodic monitoring is more appropriate for small, shallow landslides. Our application provides fast acquisition and data processing and is applicable for periodic monitoring. Also, the obtained results can be used as a high-quality input for landslide mitigation. We use achieved results as the basis for designing a GIS application in the form of a shallow landslide cadastre.

REFERENCES

[1] Bruno, F., Marillier, F.(2000). Test of high-resolution seismic reflection and other geophysical techniques on the Boup landslide in the Swiss Alps. Surveys in Geophysics 21, pp. 333-348.

[2] Bichler, A., Bobrowsky, P., Best, M., Douma, M., Hunter, J., Calvert, T., Burns, R. (2004). Three-dimensional mapping of a landslide using multi-geophysical approach: The Quesnel Forks landslide. *Landslides* 1, pp. 29-40.

[3] McGuffey, V.C., Modeer, V.A., Turner, K.A. (1996). Subsurface exploration. In: Landslides investigation and Mitigation. Special report 247, Transportation Research Board, National Research Council, National Academy Press, Washington D.C., pp. 231-277.

[4] Hack, R. (2000). Geophysics for slope stability. Surveys in Geophysics 21, pp. 423-448.

[5] Godio, A., Bottino, G. (2001). Electrical and Electromagnetic Investigation for landslide characterisation. *Physics and Chemistry of the Earth, Part C: Solar, Terrestrial & Planetary Science* 26, pp. 705-710.

[6] Lapenna, V., Lorenzo, P., Perrone, A., Piscitelli, S., Sdao, F., Rizzo, E. (2003). High resoutiongeolectricaltomographies in the study of Giarrossa landslide (southern Italy). *Bulletin of Engineering Geology and the Environment* 62, pp. 259-268.

[7] Xiujun, G., Xiaoyu, H., Yonggang, J. (2005). Forward modeling of different types of landslides with Multi-electrode electric method. *Applied Geophysics* 2, pp. 14-20.

[8] Friedel, S., Thielen, A., and Springman, S.M. (2006). Investigation of a slope endangered by rainfall-induced landslides using 3D resistivity tomography and geotechnical testing. *Journal of Applied Geophysics* 60, pp. 100-114.

[9] Marescot, L., Monnet, R., Chapellier, D. (2008). Resistivity and induced polarization surveys for slope instability studies in the Swiss Alps. *Engineering Geology* 98, pp. 18-28.

[10] Göktürkler, G., Balkaya, Ç.,Erhan, Z. (2008). Geophysical investigation of a landslide: The Altindağ landslide site, Izmir (western Turkey). *Journal of Applied Geophysics* 65, pp. 84-96.

[11] Ristić, A., Petrovački, D., Govedarica, M. (2009). A new method to simultaneously estimate the radius of a cylindrical object and the wave propagation velocity from GPR data. *Computers & Geosciences* 35, pp. 1620-1630.

[12] Sass, O., Bell, R., Glade, T. (2008). Comparasion of GPR, 2D-resistivity and traditional techniques for the subsurface exploration of the Öschingen landslide, SwabianAlb (Germany). *Geomorphology* 93, pp. 89-103.

[13] Naudet, V., Lazzari, M., Perrone, A., Loperte, A., Piscitelli, S., Lapenna, V. (2008). Integrated geophysical and geomorphological approach to investigate the snowmelt-triggered landslide of Bosco Piccolo village (Basilicata, southern Italy). *Engineering Geology* 98, pp. 156-167.

[14] Schrott, L., Sass, O. (2008). Application of field geophysics in geomorphology: Advances and limitations exemplified by case studies. *Geomorphology* 93, pp. 55-73.

[15] Sturzenegger, M., Stead, D. (2009). Close range digital photogrammetry and terrestrial laser scanning for discontinuity characterization on rock cuts. *Engineering Geology* 106, pp. 163-182.

[16] vanWesten, C., Castellanos, E., Kuriakose, S.L. (2008). Spatial data for landslide susceptibility, hazard and vulnerability assessment: An overview. *Engineering Geology* 102, pp. 112-131.

[17] Du, J.C., Teng, H.C. (2007). 3D laser scanning and GPS technology for landslide earthwork volume estimation. *Automation in Construction* 16, pp. 657-663.

[18] Rokić, L. (1997). Origins of landslides on the right bank of Danube river near Novi Sad. *International Symposium on Engineering Geology and the Environment*, Athens, June 23-27, 1997, pp. 1003-1008.

[19] Jevremović, M., Kuzmić, V. (2001). Complex geological map of Belgrade KGK 10 (1:10.000). Geozavod, Beograd.

[20] Cruden, D.M., Varnes, D.J. (1996). Landslide types and processes, in: Turner, K.A., Schuster, R.L. (eds.), Landslides investigation and Mitigation. Special report 247, Transportation Research Board, National Research Council, National Academy Press, Washington D.C., pp. 36-75.

[21] Abolmasov, B., Milenković, S., Ristić, A., Hadži-Niković, G., Đurić U. (2010). 3D terrestrial laser scanning and GPS technology for slope stability investigations-case studies. *3rd Symposium of Macedonian Association for Geotechnics*, Struga, June 24-26, pp. 2010, 9-16.

[22] Ristić, A., Petrovački, D., Govedarica, M., Popov, S. (2007). Detection of underground water flows by ground penetrating radar. *Vodoprivreda* 39, pp. 228-230, (in Serbian with English abstract).

[23] Saarenketo, T. (1998). Electrical properties of water in clay and silty soils. *Journal of Applied Geophysics* 40, pp. 73-88.